Bimodal Hydrographs in Semi-humid Forested Watershed: Characteristics and Occurrence Conditions

Zhen Cui[1], Fuqiang Tian[1*], Zilong Zhao[1], Zitong Xu[1], Yongjie Duan[1], Jie Wen[2], Mohd Yawar Ali Khan[3]

[1] Department of Hydraulic Engineering & State Key Laboratory of Hydroscience and Engineering, Tsinghua University, Beijing 100084, China.

[2] State Key Laboratory of Simulation and Regulation of Water Cycle in River Basin, China Institute of Water Resources and Hydropower Research, Beijing 100038, China.

[3] Department of Hydrogeology, Faculty of Earth Sciences, King Abdulaziz University, Jeddah 21589, Saudi Arabia.

Corresponding author: Fuqiang Tian (tianfq@tsinghua.edu.cn)

Key Points:

- The stormflow hydrograph of the studied watershed displays a bimodal pattern.

- The onset of the bimodal response demonstrates a threshold behavior.

- Delayed stormflow is mainly contributed by shallow groundwater.

Abstract

Bimodal runoff behavior, characterized by two distinct peaks in flow response, often leads to significant stormflow and associated flooding. Understanding and characterizing this phenomenon is crucial for effective flood forecasting. However, this runoff behavior has been understudied and poorly understood in semi-humid regions. In this study, we investigated the response characteristics and occurrence conditions of bimodal hydrograph based on the hydrometric and isotope data spanning 10 years in a semi-humid forested watershed in North China. The main findings include: 1) the onset of the bimodal hydrograph exhibits a threshold behavior, with delayed streamflow peaks occurring when the sum of event rainfall (P) and antecedent soil moisture index prior to the rainfall (ASI) exceeds 200 mm; 2) isotopic hydrograph separation reveals that delayed stormflow process is primarily driven by pre-event water, with increasing contributions of pre-event water during catchment wetting-up; 3) the dynamic variation in groundwater level precedes that of streamflow, establishing a hysteretic relationship wherein groundwater level peaks before streamflow during delayed stormflow. These findings, supported by onsite observations, emphasize the dominance of shallow groundwater flow in the generation of delayed stormflow.

Keywords: Semi-humid watershed, Stormflow, Bimodal runoff response, Threshold, Shallow groundwater

1. Introduction

Runoff generation is one of the most complex hydrological processes due to their complexity and non-linearity (McDonnell *et al.*, 2007; McGuire & McDonnell, 2010; Phillips, 2003). At

39   different times of a year, the activation of different runoff generating mechanisms, and contrasting

40   compartments and flow routes form different hydrograph shapes, which are generally classified as

41   unimodal and bimodal response types (Jenkins *et al.*, 1994; Gu, 1996; Kosugi *et al.*, 2011). A

42   unimodal response is characterized by a needle-shaped peak which responds immediately to the

43   rainfall impulse. In contrast, the bimodal response contains a delayed damped arch-shaped peak

44   responding to the same rainfall impulse in addition to the direct peak (Martínez-Carreras *et al.*,

45   2016). Generally, the delayed peak in a bimodal event contributes substantially more runoff than

46   the first peak (Zillgens *et al.*, 2007). For instance, the study by Onda *et al.* (2001) showed that the

47   delayed peak discharge is five to ten times greater than the first peak. When the bimodal runoff

48   event occurs, the streamflow increases markedly and lasts for several days. Therefore,

49   characterizing the bimodal response is of great significance to understanding the runoff generation

50   process and essential to achieving improved forecasting of extreme floods.

51   Since the bimodal hydrograph was accidently observed in Côte d'Ivoire in 1960 during flood

52   frequency analysis and surface runoff generation study (Dubreuil, 1960, 1985), bimodal response

53   has piqued the interest of many hydrologists worldwide and been recorded in watersheds with

54   varied geological and climate conditions. For example, Onda *et al.* (2001) observed bimodal

55   hydrographs in a steep mountainous watershed underlain by shale and serpentinite in Japan (annual

56   precipitation: 1800 mm). Padilla *et al.* (2014, 2015) found delayed peaks after the rainfall in a

57   steep headwater catchment underlain by fractured bedrock also in Japan (annual precipitation:

58   2669 mm). Zillgens *et al.* (2007) recorded a delayed peak after the direct peak in Saalach basin in

59   the Austrian Alps (annual precipitation: 1400 mm). Masiyandima *et al.* (2003) found bimodal

60   responses in an inland valley watershed with wet lowlands in central Côte d'Ivoire (annual rainfall:

61   1045 mm). Anderson and Burt (1977, 1978) observed delayed peak after the storm at Bicknoller

3

62   Combe in Sommerset, composed of impermeable Old Red Sandstone. The characteristics and

63   conditions of occurrence of bimodal hydrograph can provide an effective method for simplifying

64   the description of complex hydrological systems, and comparing stormflow generation mechanism

65   in different watersheds (Tromp-van Meerveld & McDonnel, 2006). However, most of these studies

66   mentioned above have been done in humid regions with rainfall of more than 1000 mm. To the

67   best of authors' knowledge, very few studies if not none have been conducted in semi-humid

68   environment with rainfall less than 800 mm.

69   Meanwhile, recognizing the pivotal role of bimodal response in runoff generation, researchers

70   have made concerted efforts over the past several decades to quantify its characteristics and

71   establish statistical metrics for identifying the occurrence of bimodal events. Findings suggest that

72   indicators for bimodal response encompass factors such as rainfall amount (Haga *et al.*, 2005),

73   pre-event streamflow (Graeff *et al.*, 2009), soil moisture (Anderson & Burt, 1978; Weyman, 1970),

74   groundwater level (Padilla *et al.*, 2015) and storage (Martínez-Carreras *et al.*, 2016). Taking the

75   work of Martínez-Carreras *et al.* (2016) as an illustrative example, it revealed that the delayed peak

76   manifested only when the watershed storage reached a critical threshold of 113 mm. It is

77   noteworthy that predictors vary significantly among watersheds, with only a limited number of

78   studies presenting quantitative results akin to those reported by Martínez-Carreras *et al.* (2016).

79   Moreover, response timing metrics such as response lag to peak—providing insights into different

80   aspects of water travel time during an event—have received comparatively less attention in the

81   evaluation of threshold effects (Dingman, 2015; Ross *et al.*, 2021).

82   Many studies have delved into the compartments and flow pathways responsible for

83   generating distinct runoff response patterns. The first runoff peaks are attributed to factors such as

84   rainwater directly falling onto the stream channel, rapid flow through preferential paths (Becker

4

85   & McDonnell, 1998; Martínez-Carreras *et al.*, 2015; Wrede *et al.*, 2015), or saturation-excess

86   overland flow in the riparian zone (Anderson & Burt, 1978; Westhoff *et al.*, 2011). While delayed

87   runoff peaks in bimodal events are primarily linked to subsurface flow processes (Weyman, 1970;

88   Onda *et al.*, 2006; Zillgens *et al.*, 2007; Graeff *et al.*, 2009; Padilla *et al.*, 2015). However, a notable

89   gap exists in the literature, as many studies have focused solely on water flow processes within the

90   soil profile without thoroughly investigating whether subsurface stormflow originates from the

91   soil layer, bedrock layer, or a combination of both.

92   　　Bimodal responses, representing the nonlinear interplay between runoff and rainfall,

93   inherently showcase the stormflow process in terms of both response timing and magnitude. This

94   intuitive manifestation holds significant implications for advancing runoff modeling (Graeff *et al.*,

95   2009; McDonnell *et al.*, 2007) and enhancing the precision of flash flood forecasting (Zhang *et al.*,

96   2021; Zillgens *et al.*, 2007). In our present study, spanning the years 2014 to 2023, we collected

97   data on rainfall, groundwater levels, soil water content, and streamflow within a semi-humid forest

98   experimental watershed in North China. Our investigation involves characterizing the response

99   magnitude and timing of stormflow to rainfall through hydrograph analysis, while also scrutinizing

100   the composition of the water sources contributing to stormflow. Specifically, we hypothesize that

101   (1) the occurrence of bimodal streamflow responses exhibits a threshold behavior with rainfall and

102   watershed wetness, and (2) the primary source of water for the delayed stormflow is subsurface

103   flow.

2. Materials and Methods

2.1 Study area

The study headwater catchment, the Xitaizi Experimental Watershed (XEW), is situated at coordinates 40°32′N and 116°37′E, as depicted in Figure 1. Spanning an area of 4.22 km², XEW exhibits elevations ranging from 676 to 1201 m above sea level. Approximately 54% of the area features a slope between 20% and 40%. The region experiences a monsoon-influenced semi-humid climate characterized by an average annual rainfall of 625 mm. The majority of this precipitation, around 80%, occurs between June and September. The annual mean temperature in the area is 11.5°C, accompanied by a relative humidity of 59.1%. Experimental and observational activities were conducted over the period from 2014 to 2023.
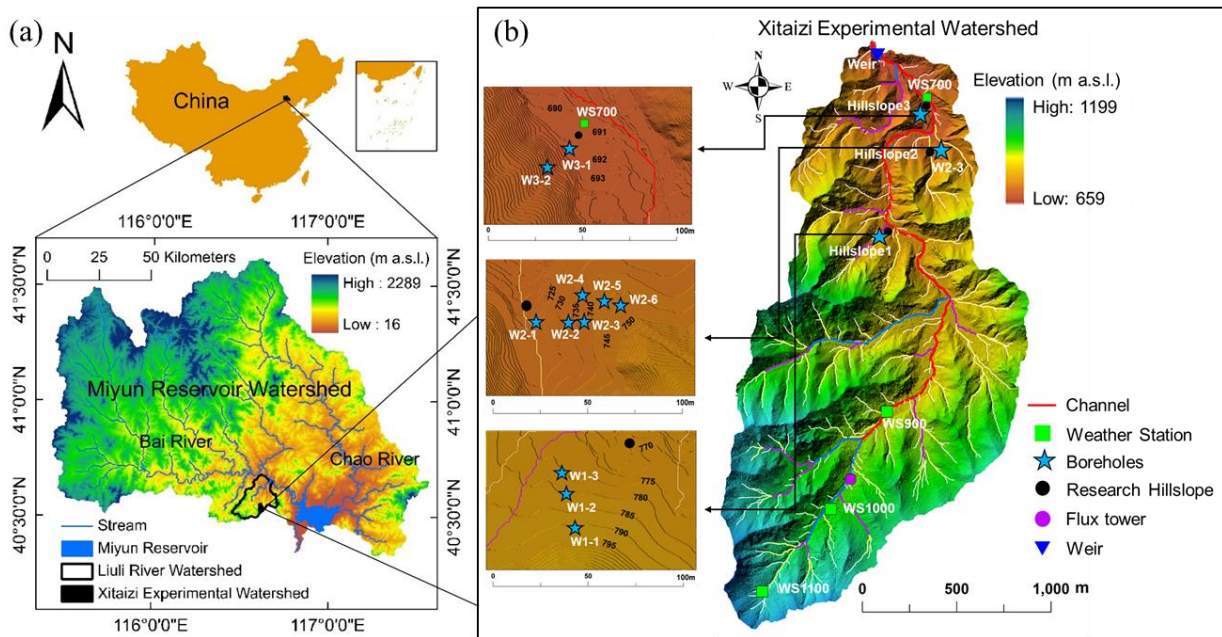
Figure 1. Location of the Xitaizi Experimental Watershed (XEW) in North China (a), and the detailed distributed monitoring stations and instruments (b), including four automatic weather stations (WS700-1100), one weir, and eleven groundwater boreholes (blue star corresponds with well numbers and locations). Four rain gauges are located near the weather stations, and one is located adjacent to the weir.

6

121   XEW represents a typical location in North China's earth-rocky mountainous region, where

122   approximately 80% of the catchment area is underlain by firmly compacted, deeply weathered

123   granite. Soil mapping and field investigations reveal the prevalent soil types to be brown earth and

124   cinnamon soil (according to Chinese soil taxonomy), with a depth extending to 1.5 meters. The

125   saturated hydraulic conductivity of the soil ranges from 19.5 to 175.3 mm/h, with an average value

126   of 45 mm/h. The bedrock in the area is primarily composed of granite, constituting approximately

127   88% of the total bedrock composition, while gneiss and dolomite are sporadically distributed.

128   Some sections of the granite exhibit fracture, and a layer of regolith is sandwiched between the

129   soil layer and the bedrock layer. In terms of land cover, the catchment is predominantly covered

130   by forest (98%), with 54.2% being broad-leaved, 2.3% coniferous, and 10.5% a mix of coniferous

131   and broad-leaved. The remaining 33% consists of shrubs (Tie *et al.*, 2017).

132   **2.2 Meteorology and runoff measurements**

133   Meteorological variables and runoff have been systematically monitored since 2013.

134   Meteorological conditions were consistently measured using four GRWS100 automatic weather

135   stations. These weather stations were strategically distributed quasi-uniformly along the elevation

136   gradient, as depicted in Figure 1. The comprehensive data collection from these stations

137   contributes to a thorough understanding of the meteorological dynamics in the study area over the

138   specified timeframe.

139   For the measurement of air temperature (*Ta*) and relative humidity at each automatic weather

140   station, an HC2S3-L temperature and relative humidity probe was utilized. These probes were

141   equipped with a radiation shield to enhance accuracy. Simultaneously, a LI-190R quantum sensor

142   was employed to measure photosynthetically active radiation (PAR). Rainfall data were collected

143   at 10-minute intervals using six tipping-bucket rain gauges. These gauges were positioned in an

144   open space near the automatic weather stations, and average values were adopted for analysis in

145   this study.

146   Furthermore, the antecedent precipitation index (API), generally used to represent the residual

147   effect of previous precipitation (Mosley, 1979; Iwagami *et al.*, 2010), was calculated for all the

148   events over 3, 6, and 12 days. The API during the antecedent *t* days is described as follows:

149    $$\text{API}\,(t) = \sum_{i=1}^{t} \frac{P_i}{i} \tag{1}$$

150   where i is the day count and P_i is the daily precipitation in the ith day previously.

151   A Parshall flume was installed at the catchment outlet to measure streamflow (Figure 1). The

152   water level in the flume was measured every 5 min with a HOBO capacitance water level logger

153   from 2014. Streamflow was calculated using the standard Parshall flume rating curve, and both

154   the rainfall and streamflow measurements were averaged to hourly timesteps, and in this study,

155   the analysis is conducted at hourly timesteps. Unfortunately, the observation equipment is

156   susceptible to failures due to the complex environmental conditions and disturbances caused by

157   wild animals and plants. Compounded by the remote location of XEW, accessing the site promptly

158   to address malfunctions is challenging, leading to the loss of some observation data. Notably,

159   stormflow data from July 19 to August 16, 2016, had to be excluded because the road collapsed

160   during a heavy storm, preventing a significant amount of runoff from passing through the Parshall

161   flume. Furthermore, streamflow data from 2018 to 2019 are unavailable, and the two bimodal

162   events in 2016 were omitted from the hysteresis analysis due to substantial errors in streamflow

163   observations resulting from damage to the diversion channel. The specific observation periods are

164   detailed in Table 1. These limitations underscore the challenges associated with conducting

165   observations in remote and environmentally intricate locations.

Table 1. Rainfall-runoff event classification and counts by year. This table provides a breakdown of the number of rainfall-runoff events categorized as unimodal, bimodal, and hybrid bimodal for each year, along with the corresponding time periods. The total counts are summarized at the bottom.

Year	Unimodal event	Bimodal event	Hybrid bimodal event	Time period
Characteristics	A needle-shaped peak which responds immediately to the rainfall impulse	A delayed damped arch-shaped peak responding to the same rainfall impulse in addition to the direct peak	The delayed peak increased rapidly and merged with the direct peak, generating extremely high streamflow volume	
2014	7	-	-	Jul 25 - Sep 25
2015	12	2	-	Jun 1 - Oct 1
2016	2	2	1	Jul 10 - Aug 20
2017	-	2	-	Jun 20 - Jul 10
2020	14	2	-	Jul 1 - Oct 10
2021	15	5	2	Jun1 - Oct 10
2022	18	1	-	Apr 1 - Nov 1
2023	9	-	1	Apr 1 - Nov 1
Total	77	14	4	

2.3. Soil water content observation

Volumetric soil water content (SWC) was measured at eight observation sites using CS616 time-domain reflectometry (TDR) probes at 10-min intervals. ~~These measurements were taken at 10-minute intervals.~~ On Hillslope 1, five soil moisture sensors were deployed, with an additional three located adjacent to WS900. These sensors were strategically placed in the soil profiles at 80 cm depth intervals, each at a depth of 10 cm. For analysis in this study, the 10-minute interval measurements were aggregated to hourly time steps, and the arithmetic mean of the total SWC across the four profiles was employed. Moreover, SWC data immediately preceding a rainfall event were integrated over the 80 cm depth to calculate an antecedent soil moisture index (ASI), as proposed by Haga *et al.* (2005). This index, commonly utilized in analyzing the impact of

181   antecedent shallow soil water storage on catchment runoff response (Fu *et al.*, 2013; Penna *et al.*,

182   2011), provides valuable insights into the soil moisture conditions preceding rainfall events.

183   **2.4 Groundwater level observation**

184   Fluctuations in groundwater level (below the ground surface, hereinafter referred to as bgs)

185   were systematically recorded in eleven 80 mm diameter boreholes situated on three hillslopes

186   within the catchment (refer to Figure 1). The boreholes were drilled to depths of 5-26 m in granite

187   (weathered and fractured to varying extents) mantled by thin soils. Unscreened portions of the

188   boreholes accounted for approximately one third to three fifths of the total depth (refer to Table 2).

189   To capture the groundwater level dynamics, HOBO capacitance water level loggers (Onset, USA)

190   were deployed to record water levels in the boreholes at hourly intervals. It is noteworthy that

191   water levels were rarely observed in boreholes W1-1, W1-2, W2-4, W2-5, and W2-6. This

192   observation could be attributed to the boreholes potentially not being drilled deep enough to reach

193   the groundwater, possibly due to challenges encountered during field drilling. Slug tests conducted

194   following installation suggested that the saturated conductivity in the weathered and fractured

195   granite was relatively high, ranging from 5.2×10^{-3} m/day to as high as 1.16 m/day.

196

197

198

199

200

201

Table 2. Depths and groundwater levels of boreholes. This table summarizes the depths of the bottom and the boundary between unscreened and screened portions, along with the shallowest and deepest groundwater levels of boreholes in the study area.

Borehole	Bottom (m)	Boundary (m)	Shallowest GWL (m)	Deepest GWL (m)
W1-3	10	6	2.8	10[a]
W2-1	5	2	0.2	2.2
W2-2	10	4	4.8	10[a]
W2-3	26	9	6.4	12.2
W3-1	10	4	0.8	3.9
W3-2	10	4	6.1	9.9

Note: All values indicate depths (in meters) from the ground surface; GWL represents groundwater level; 'a' indicates the groundwater level dropped below the bottom of the borehole.

An index for groundwater level (I_G) was computed by normalizing the groundwater levels in each borehole to their recorded range throughout the research years, following the approach outlined by Detty and McGuire (2010). Subsequently, the arithmetic mean of I_G across all boreholes was calculated, serving as a representative proxy for the groundwater level across the entire catchment. This approach provides a standardized measure that allows for the comparison of groundwater level variations across different boreholes within the study area.

2.5 Separation of rainfall-runoff events

An intensity-based automatic algorithm, as outlined by Tian *et al.* (2012) and Powell *et al.* (2007), was employed to delineate and segregate rainfall events from hourly rainfall time series data. In this algorithm, a threshold rainfall intensity of >0.1 mm/h was utilized to determine the commencement and conclusion of each event, with individual storms being separated by a minimum of six hours. Events characterized by an accumulated rainfall exceeding 5 mm were selected for further analysis. A total of 95 distinct rainfall events, each with a cumulative rainfall of at least 5 mm, were identified and isolated from the rainfall data series spanning the years 2014 to 2023, employing the intensity-based automatic method (refer to Table 1).

223   Storm runoff events are identified when streamflow experiences a rapid increase and attains

224   a peak in response to a rain impulse. Throughout the analyses presented, streamflow refers to the

225   total discharge measured at the weir. The computer program HYSEP (Sloto & Crouse, 1996) was

226   employed to automatically partition a streamflow hydrograph into baseflow and stormflow

227   components. Subsequently, the automated separation outcomes underwent manual verification and

228   adjustment, aligning with observed data and widely accepted straight-line separation principles. In

229   the context of each event, q_0 is defined as the streamflow before the onset of rainfall. This

230   parameter characterizes the baseflow conditions preceding the hydrograph's response to a rain

231   impulse (Zillgens *et al.*, 2007). The separation of stormflow from base flow allows for a more

232   detailed examination of the runoff dynamics during distinct rainfall events.

233   **2.6 Hydrograph and event types**

234   The hydrograph served as a valuable tool for characterizing the timing, magnitude, and

235   duration of runoff responses to rainfall. ~~Two~~ Three primary response types were identified based

236   on the number and shape of streamflow peaks: unimodal, bimodal and hybrid bimodal events.

237   Schematic diagrams illustrating these three types of events are presented in Figure 2.

238   A unimodal event has a single peak generates during or shortly after the cessation of rain

239   impulse (refer to Figure 2a). While a bimodal event features two peaks as a response to the same

240   rain impulse, of which the direct peak (also called the first peak) corresponds to a fast catchment

241   response to rainfall and occurs synchronously with the rainfall or shortly after its onset.

242   Additionally, we referred those events has a similarly shaped hydrograph to unimodal event, but

243   the water yield and peak delay time are significantly greater, as hybrid bimodal events. Hybrid

244   bimodal events can be distinguished from unimodal events by their extremely high streamflow

12

245   volume, longer duration, and delayed response time (Figure 2c). The hydrographs of bimodal and

246   hybrid bimodal events can refer to Figures 12 ~~and 13~~.

247   It's worth noting that a rainfall event may consist of multiple impulses, and in such cases, the

248   hydrograph responds with multiple direct peaks (see Figure 2b). The stormflows from the first

249   peak (q_{1p}) and delayed peak (q_{2p}), along with the total event stormflow ($qs = q_{1p} + q_{2p}$), were

250   calculated by summing hourly values over the identified event period. The runoff ratio (Rr),

251   commonly used to estimate the effective contributing area during a runoff event (Buttle $et\ al.$, 2004;

252   Detty & McGuire, 2010), is calculated as the ratio of qs to gross rainfall.
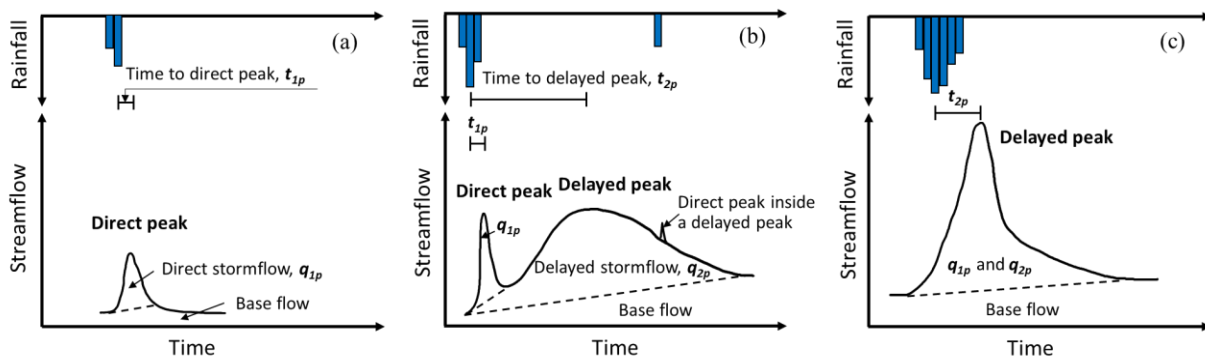
253

254   **Figure 2.** Schematic diagrams of the hydrographs of an (a) unimodal event, (b) typical bimodal
255   events, and (c) hybrid bimodal event (modified from Zillgens $et\ al.$, 2007).

256

257   **2.7 Definition of lag time**

258   The lag time, defined as the duration between peak rainfall and peak streamflow (Mosley,

259   1979), is a critical parameter for modeling the temporal variability of streamflow. Lag time varies

260   significantly among different water sources (Becker, 2005; Haga $et\ al.$, 2005) and has been

261   introduced to comprehend sub-components of runoff in different response processes. In this study,

262   two specific lag times are considered: t_{1p} the time lag between peak rainfall intensity and the first

263   streamflow peak, and t_{2p} the time lag between peak rainfall intensity and the delayed streamflow

264   peak, as illustrated in Figure 2.

265   **2.8 Water sampling and isotope analysis**

266   Water samples for isotope analysis ($\delta^{18}O$ and δD) were collected from July 1 to September 1,

267   2021. Rainwater was automatically sampled every two hours using an ISCO6712 automatic water

268   sampler (Inc., Lincoln, Nebraska, USA) positioned near the weir. Manual bulk samples of rainfall

269   were also collected at the same location after each event using a rainwater sampler with a 9.5 cm

270   diameter funnel attached to a 500 ml plastic water bottle, insulated with bubble foil to protect

271   against direct sunlight, and a table tennis ball placed in the funnel's mouth to minimize evaporation.

272   Stream water was collected every two hours upstream of the Parshall flume location using an

273   automatic water sampler (Figure 1). Spring, seepage water, and groundwater were manually

274   collected daily from boreholes using a bailer. All collected samples underwent isotopic

275   composition analysis ($\delta^{18}O$ and δD) using a Picarro L2140-i isotopic liquid water and water vapor

276   analyzer (wavelength-scanned cavity ring-down spectroscopy, WS-CRDS) with a declared

277   precision of $\delta^{18}O \pm 0.1$‰ and $\delta D \pm 1$‰.

278   **2.9 Isotopic hydrograph separation**

279   To trace the source of the streamflow during storm events, a simple mass balance approach

280   was employed to segregate the streamflow into two components: event water and pre-event water.

281   These components are represented by rainfall and baseflow, respectively, based on the oxygen

282   isotopic concentration ($\delta^{18}O$) of each component. The $\delta^{18}O$ of baseflow and weighted rainwater

283   samples served as end members, defining the ultimate isotopic composition of the stream, in

284   accordance with the approach outlined by Padilla *et al.* (2014):

285    $$C_s = xC_e + (1 - x)C_p \qquad (2)$$

14

$$x = \frac{C_s - C_p}{C_e - C_p} \cdot 100 [\%] \tag{3}$$

where C_s, C_e and C_p refer to δ^{18}O concentrations of stream, event and pre-event water components, respectively. C_e is the weighted value calculated using the incremental mean weighting method (McDonnell *et al.*, 1990) for each event. C_p is determined from the stream δ^{18}O concentration measured immediately preceding the rainfall. x is the percentage of event water in stream.

3. Results

3.1 Characteristics of different runoff response types

During the period from 2014 to 2023, a total of 95 distinct rainfall events, each with a cumulative rainfall of at least 5 mm, were identified from the rainfall data series. Among these events, 14 exhibited a bimodal response, and an additional 4 displayed a hybrid bimodal process (refer to Table 1).
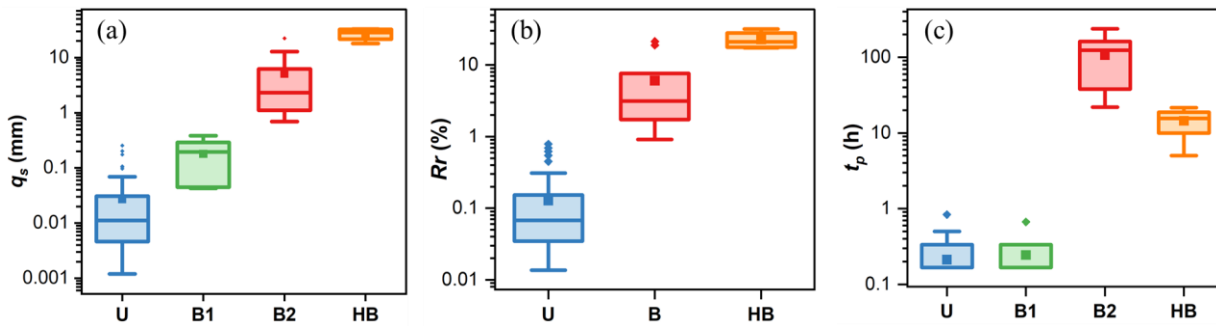
Figure 3. Comparison of (a) stormflow, q_s, (b) runoff ratio, Rr and (c) lag time (t_p) from peak rainfall to peak streamflow of different event types. U indicates unimodal event, B (including the first peak B1 and the delayed peak B2) bimodal event and HB hybrid bimodal event. In each boxplot, the lower and upper limits represent the lower and upper quartiles, while the whiskers extend to the minimum and maximum values in each dataset. The horizontal line within the box signifies the median. Individual asterisks denote points more than 1.5 times away from the median. It's noteworthy that a semi-logarithmic coordinate was utilized for enhanced interpretability due to the extensive range.

15

307   The stormflow volume and lag times of streamflow peaks for both unimodal and bimodal

308   events were determined and characterized. As depicted in Figure 3, unimodal events generated

309   relatively minimal runoff, with a maximum q_{1p} of 0.25 mm. In contrast, the q_{1p} and q_{2p} of bimodal

310   events exhibited a wider range, spanning from 0.03 to 0.38 mm and from 0.82 to 31.63 mm,

311   respectively (Figure 3b). The stormflow volume of bimodal events proved to be 3 to 114 times

312   larger than that of unimodal events, primarily due to the presence of delayed peaks (Figure 3a).

313   Correspondingly, bimodal events displayed higher Rr values ranging from 0.91% to 31.81%,

314   whereas the Rr of unimodal events remained below 0.8% (Figure 3b). This discrepancy suggests

315   an expanded effective contributing area during bimodal and hybrid bimodal events, as highlighted

316   in previous studies (Zhang *et al.*, 2021).

317   In both unimodal and bimodal events, all direct peaks were observed within a one-hour

318   timeframe. However, the delayed peak, a distinctive feature of bimodal events, manifested itself

319   between 5 hours and 9.9 days after the occurrence of the direct peak. Notably, hybrid bimodal

320   events exhibited shorter lag times and significantly higher stormflow yield, underscoring the need

321   for heightened attention in flood forecasting. The substantial difference in lag time strongly implies

322   that these peaks are contributed by distinct water sources, aligning with findings from previous

323   studies (Haga *et al.*, 2005).

324   **3.2 Determinants of delayed streamflow peaks**

325   The relationships between different event types and rainfall characteristic parameters and

326   watershed wetness indicators were further depicted in Figure 4. It is noteworthy that the soil water

327   content (SWC) and groundwater level index (I_G) presented in Figure 4 represent data recorded at

328   the end of rainfall events, considering that delayed streamflow peaks typically manifest subsequent

329   to the cessation of rainfall events. Rainfall amount, I_G, and SWC were statistically significantly

16

330 different for both groups, as proven by the t-test of equality of medians at a significance level of

331 α=0.01. The transition from unimodal to bimodal events reveals a consistent increase in rainfall

332 amount, I_G, and SWC. Nearly all bimodal events exhibited rainfall amounts exceeding 50 mm,

333 whereas the range for unimodal events varied from 5.2 to 66.6 mm (Figure 4a). This suggests that

334 the initiation of delayed streamflow peaks may be associated with substantial rainfall.

335   The I_G and SWC of bimodal events, especially hybrid bimodal events, were significantly

336 higher (p < 0.01) than those of unimodal events. Despite partial overlap in the ranges of I_G and

337 SWC for these groups (Figure 4d and e), the mean I_G and SWC values for bimodal events (0.46

338 and 0.67) were notably greater than those for unimodal events (0.22 and 0.13), underscoring the

339 distinctiveness of these parameters between event types. Contrastingly, peak rainfall intensity,

340 mean rainfall intensity, and Antecedent Precipitation Index (API) metrics (API3, API6, and API12)

341 exhibited a widespread overlap in their variation (p > 0.05, Figure 4b, d, g-i). Consequently, while

342 bimodal events were characterized by higher rainfall and antecedent wetness, I_G and SWC emerged

343 as more effective indicators for estimating the occurrence of bimodal events, while peak rainfall

344 intensity, mean rainfall intensity, and API were found to be insufficient for distinguishing between

345 bimodal and unimodal events.
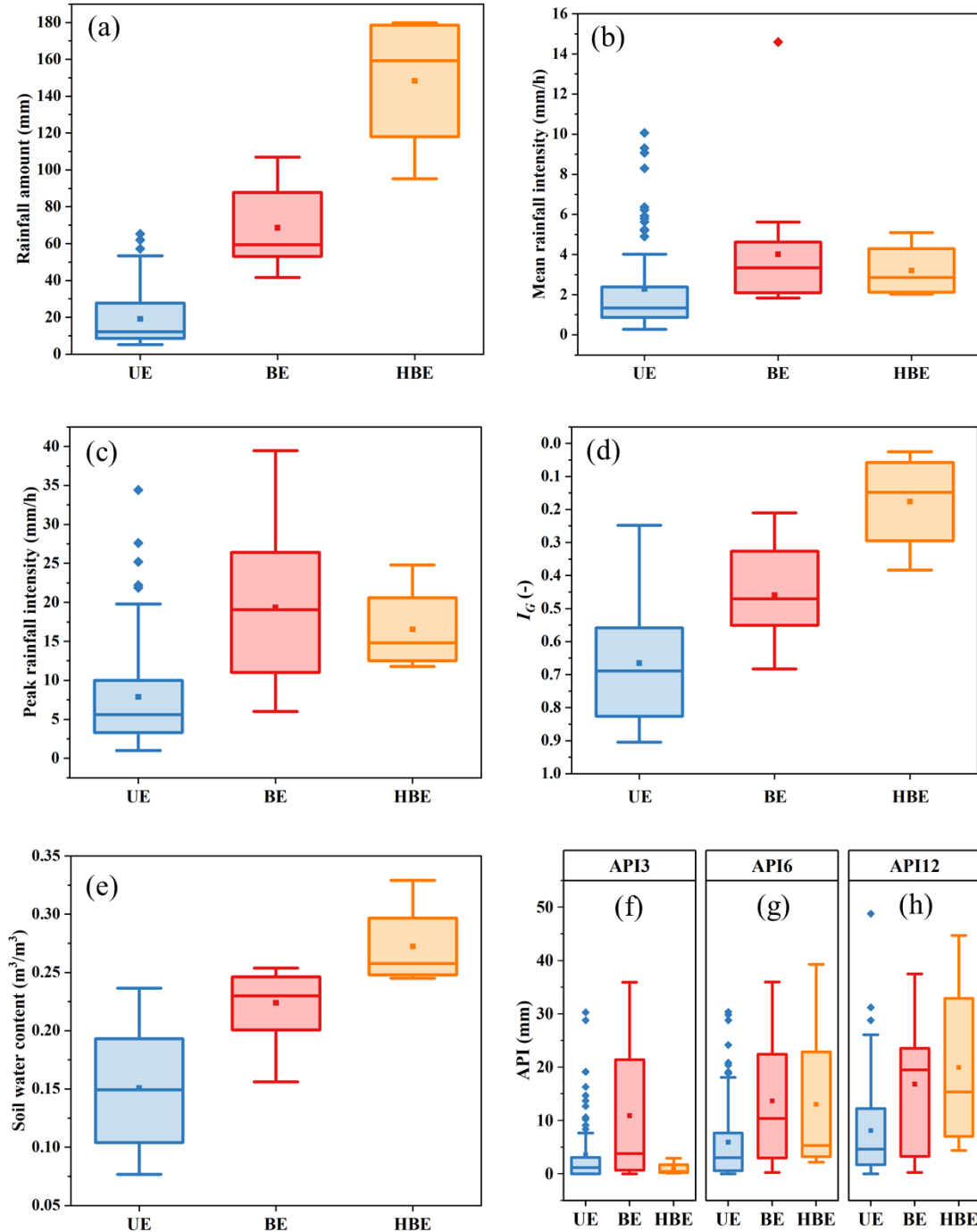
346
347 **Figure 4.** Box plots of the hydrological characteristic parameters for unimodal and bimodal events.
348 (a) rainfall amount; (b) mean rainfall intensity; (c) peak rainfall intensity; (d) I_G: groundwater level
349 index; (e) soil water content; (g)-(i) API3, API6 and API12: antecedent precipitation index over 3,
350 6 and 12 days. UE, BE and HBE are respectively unimodal, bimodal and hybrid bimodal events.
351 To be noted, each element of the box carries the same interpretation as described in Figure 3.
352

353   Considering the interdependence of groundwater level, streamflow, and SWC on rainfall, a

354 detailed examination of the relationship between rainfall amount and bimodal events was

355 conducted. The analysis revealed that the occurrence of delayed peaks is contingent on both event

356 rainfall and antecedent wetness, displaying a distinct threshold behavior (Figure 5b). The

357 combined sum of event rainfall amount (P) and antecedent soil moisture index prior to the rainfall

358 (ASI_0) serves as a reliable indicator for predicting the occurrence of delayed peaks. Figure 5

359 illustrates that bimodal events tend to manifest when $P + ASI_0$ exceeds 200 mm (with only two

360 bimodal events misplaced). An intriguing observation is that these misplaced bimodal events

361 produced very little q_s, and these unimodal events nearby to the threshold, occurred just before the

362 year's first bimodal response when the watershed was sufficiently humid, signaling a

363 predisposition for bimodal events. However, once the rainfall surpassed the threshold, all bimodal

364 episodes were randomly distributed, and no discernible relationship was observed between their

365 stormflow volume (q_s) and rainfall amount. Based on these findings, we posit that the stormflow

366 generation process may be dominated by groundwater or SWC.

367
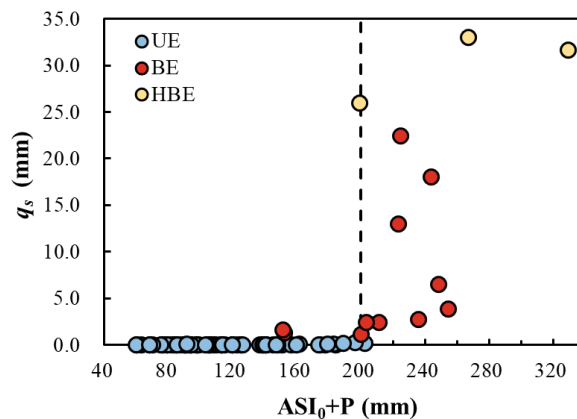
Figure 5. Relationship between the $ASI_0 + P$ and stormflow volumes (q_s) of different event types.
UE is unimodal event, HBE is hybrid bimodal event, P is rainfall amount, and ASI_0 is antecedent
soil moisture index before the rainfall.

371

19

3.3 Timing of groundwater, soil water, and streamflow response

The preceding analysis indicates a correlation between different event types and groundwater levels along with SWC. Moreover, the inconsistent response time among different event types may signify distinct contributing sources to the stream channel, providing insights into the primary mechanisms behind runoff generation. Earlier or identical response timing of groundwater compared with streamflow suggested that streamflow response was driven by hillslope groundwater (Haught and Meerveld, 2011; Rinderer *et al*., 2016). To explore this further, six bimodal events with minimal or sporadic rainfall during the delayed peak period, along with three unimodal events, were selected. The response timing of groundwater, SWC, and streamflow is illustrated in Figure 6. Each horizontal bar represents the onset of rain on the left end and the lag time for the peak value on the right end of the corresponding variable. It's worth noting that some groundwater levels in Figures 6d, e, and g lack horizontal bars due to missing groundwater level data, while the groundwater levels in Figure 6c lack horizontal bars due to no response from groundwater.

SWC reached their maximum after direct streamflow peaks but before delayed peaks. Particularly in typical bimodal events, SWCs peaked much earlier than delayed streamflow peaks, suggesting that, in these events, soil water did not contribute to direct peak but may to delayed streamflow peaks. Regarding groundwater levels, some locations showed two peaks and not all responded to the same rainfall event. Among different locations, groundwater levels peaked before or after the delayed streamflow peaks. However, for the hybrid bimodal events, the response time of groundwater levels at various locations, and even the SWC tended to coincide with the delayed streamflow peak. Identical response timing or groundwater rising and peaking just before the stream suggest that whole catchment or critical zone contributed to delayed stormflow.
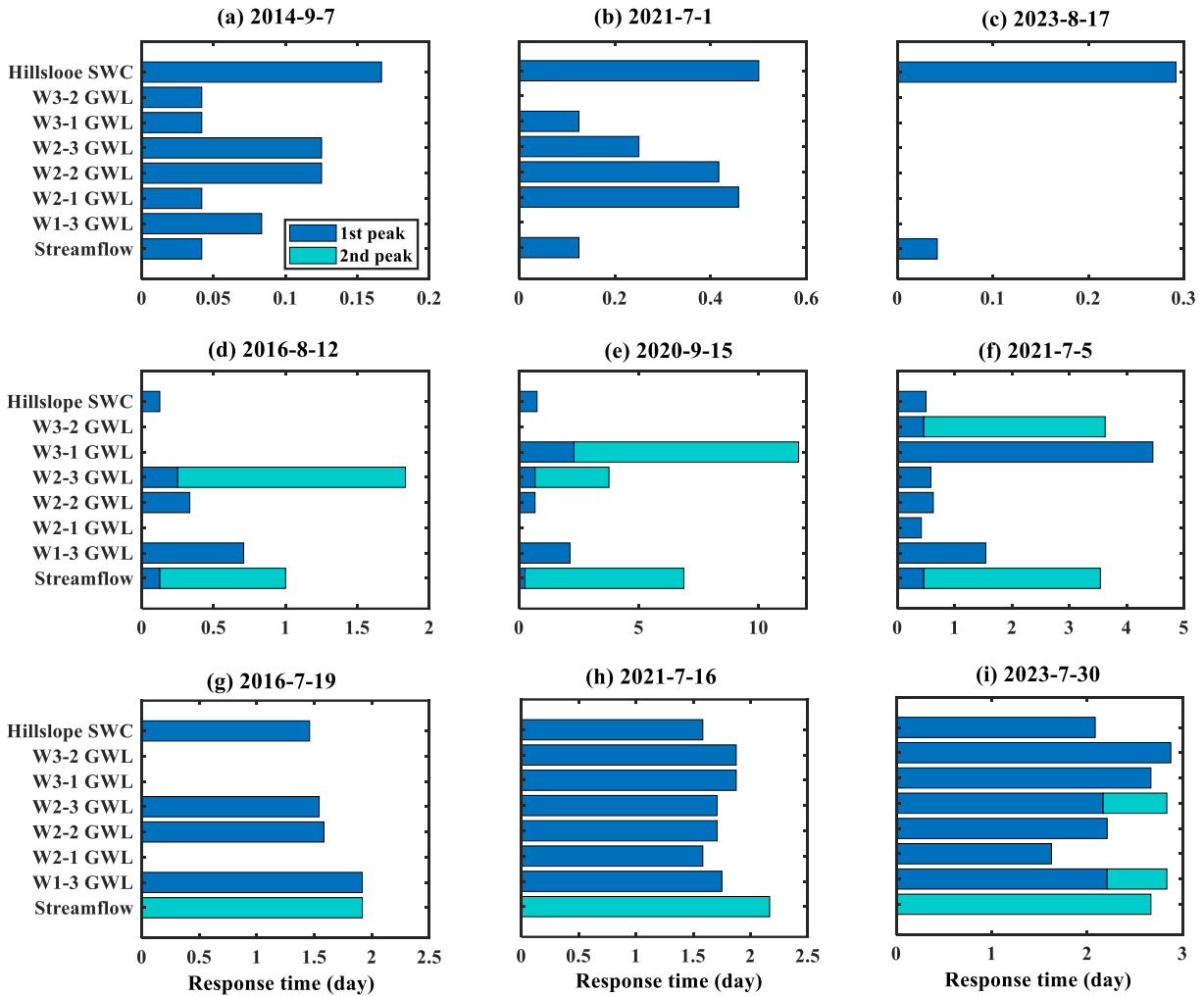
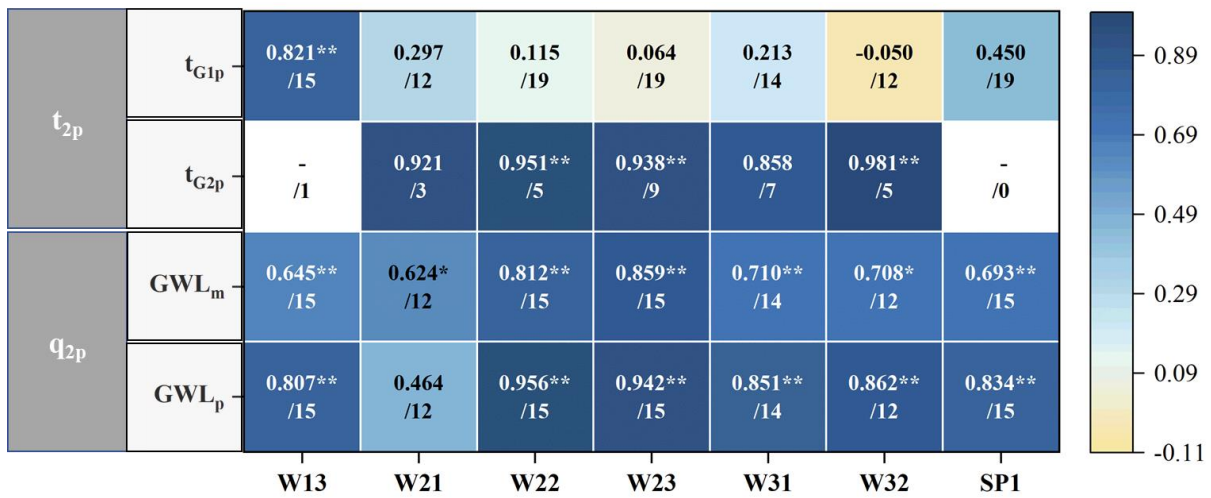**Figure 6.** Response time of streamflow, groundwater level and soil water content in nine events. The horizontal axis illustrates the lag time from the onset of rainfall. The bar lengths depict the time taken for volumetric water content and groundwater level to reach their respective maximums from the onset of rainfall. GWL is groundwater level, and SWC is soil water content. Each row and column chart shares identical vertical and horizontal axis titles.

Pearson correlation coefficients (r_p) between peak groundwater levels, peak SWC and delayed streamflow were calculated for 19 bimodal events. As showed in Figure 7, the first two lines show the correlation coefficients between t_{2p} and the lag time of the peak groundwater levels and SWC, t_{G1p} and t_{G2p} represent the response times of the first and second peaks of groundwater level or SWC, respectively. The last two lines show the correlation coefficients between q_{2p} and

21

the average and peak values of groundwater levels and SWC. The number after the slash specifies

407 how many pairs of the variables.

408 Groundwater levels exhibited two peaks in some events, with the exception of W13.

409 Correspondingly, among these events, the response time of the second peak of groundwater level

410 has a strong correlation with t_{2p} with the $r_p > 0.858$. Even though W13's groundwater level only

411 has one peak, this peak's response time was highly correlated with t_{2p} at the 0.01 significance level

412 ($r_p = 0.821$). In contrast, SWC displayed one peak in all events, and its response time exhibited a

413 weak correlation with t_{2p} ($r_p = 0.450$). Both groundwater levels and SWC, particularly their peak

414 values, demonstrated a high correlation with delayed stormflow volumes (q_s). Above all,

415 groundwater is deemed to be the primary controlling factor in delayed stormflow.

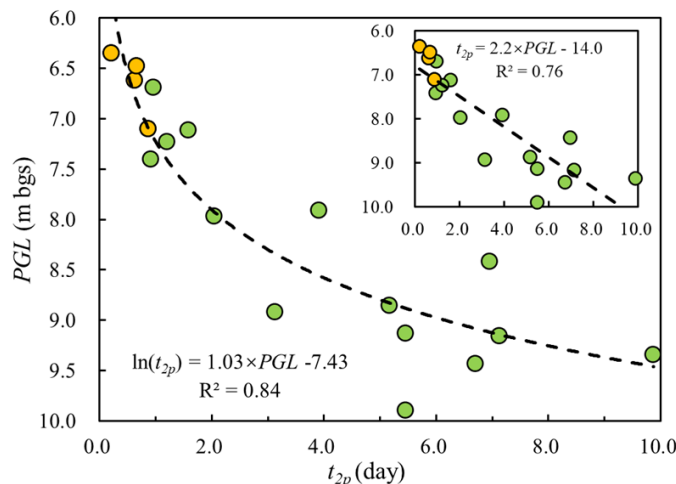|		W13	W21	W22	W23	W31	W32	SP1
t_{2p}	t_{G1p}	0.821** /15	0.297 /12	0.115 /19	0.064 /19	0.213 /14	-0.050 /12	0.450 /19
	t_{G2p}	- /1	0.921 /3	0.951** /5	0.938** /9	0.858 /7	0.981** /5	- /0
q_{2p}	GWL_m	0.645** /15	0.624* /12	0.812** /15	0.859** /15	0.710** /14	0.708* /12	0.693** /15
	GWL_p	0.807** /15	0.464 /12	0.956** /15	0.942** /15	0.851** /14	0.862** /12	0.834** /15

416

417 Figure 7. Pearson correlation coefficients between peak streamflow and peak groundwater levels.
418 The number after the slash specifies how many pairs of the variables. I_G, groundwater water level
419 index; ** Denotes that correlation is significant at the 0.01 level (two-tailed).
420
421 The robust correlation observed between groundwater levels at different locations and

422 stormflow suggests that groundwater observations at a specific location can serve as a

423 representative proxy for the overall groundwater level across the watershed. Given the relatively

424   complete and dynamic water level observation data for W23, this borehole was selected for further

425   analysis.

### 3.4 Stormflow timing and magnitude characteristics

427   Considering the high correlation between streamflow and groundwater level as indicated in

428   the previous analysis, we hypothesized a connection between groundwater and delayed stormflow.

429   To elucidate this correlation between groundwater and streamflow, we fitted the relationship

430   between the groundwater level at location W23 and the magnitude and timing of the delayed

431   stormflow for bimodal events. The time lag of delayed peak (t_{2p}) shows a negative exponential

432   correlation with peak groundwater level ($ln(t_{2p}) = 1.03 \times PGL$ - 7.43, $R^2 = 0.84$, $p < 0.01$, Figure

433   8), suggesting that a higher groundwater level corresponds to a faster response of the delayed

434   runoff peak to rainfall. A comparable linear correlation was also fitted between t_{2p} and groundwater

435   level, albeit with a slightly lower R^2 ($R^2 = 0.76$).

Figure 8. Correlation between peak groundwater level (*PGL*) and lag time of the delayed
streamflow peak (t_{2p}). The insert shows the same plot with linear fitting. Orange solid circles
represent hybrid bimodal events.

440   Moreover, as shown in Figure 9, q_s also has a strong linear relationship with groundwater

441   level ($q_s = -10 \times PGL + 94.8$, $R^2 = 0.91$, $p < 0.01$). These results highlight the significant influence

23

442 of groundwater on flood generation in the studied watershed, suggesting that incorporating

443 groundwater level variations into flood forecasting models could enhance their accuracy.
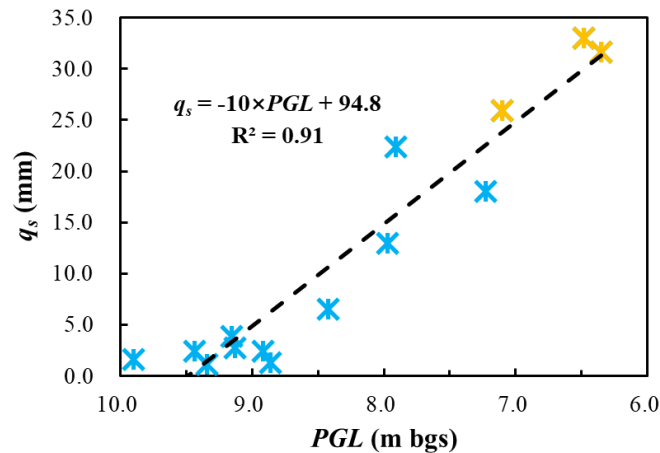

444

445 **Figure 9.** Correlation between peak groundwater (*PGL*) level and stormflow amount (q_s) for
446 bimodal events. Orange stars represent hybrid bimodal events.

447   For both fitted lines, the closely matching fitting lines for hybrid bimodal events support the

448 hypothesis that these high, delayed streamflow responses, which may appear unimodal, are, in fact,

449 bimodal. During hybrid bimodal events, the delayed peak increased rapidly and reached its peak

450 within one day, practically merging with the direct peak. This led to a potentially misleading result

451 that only one peak was generated. This occurrence was likely due to the groundwater level rising

452 rapidly to a critical level with substantially higher hydraulic conductivity, allowing a larger portion

453 of the hillslope to become hydraulically connected to the stream during these events within a very

454 short time. Consequently, a substantial amount of groundwater was quickly discharged into the

455 channel.

456 **3.5 Isotope composition of groundwater and stream water**

457   To gain additional insight into the control of groundwater level on delayed stormflow, the

458 isotope compositions of different water bodies were analyzed. Figure 10 summarizes the $\delta^{18}O$ of

459 stream, spring, seepage water and the groundwater $\delta^{18}O$ from all boreholes between July 1 and

24

460 September 1 in 2021. Rainwater exhibited a high variation in $\delta^{18}O$ composition (ranging from -

461 14.42 to -5.28 ‰), with a rainfall-weighted mean $\delta^{18}O$ value of -9.197. In contrast, groundwater

462 $\delta^{18}O$ composition appeared more stable throughout the sampling period, showing little variation

463 across various boreholes, with a mean $\delta^{18}O$ value ranging from -9.76±0.10 to -9.08±0.86‰. This

464 stability indicates minimal event-based mixing with rainwater. The $\delta^{18}O$ values of spring and

465 seepage water followed a pattern similar to that of groundwater. The average $\delta^{18}O$ value of the

466 stream (-9.51‰) closely resembled that of groundwater (-9.49‰). Although the stream's $\delta^{18}O$

467 composition briefly deviated toward that of rainfall during a storm, it quickly reverted to its

468 previous value, resembling groundwater. Large isotopic variation in rainfall was dampened in the

469 stream, indicating that both baseflow and some stormflow originated from groundwater storage

470 with a consistent isotopic ratio, a result of dispersion and mixing processes.
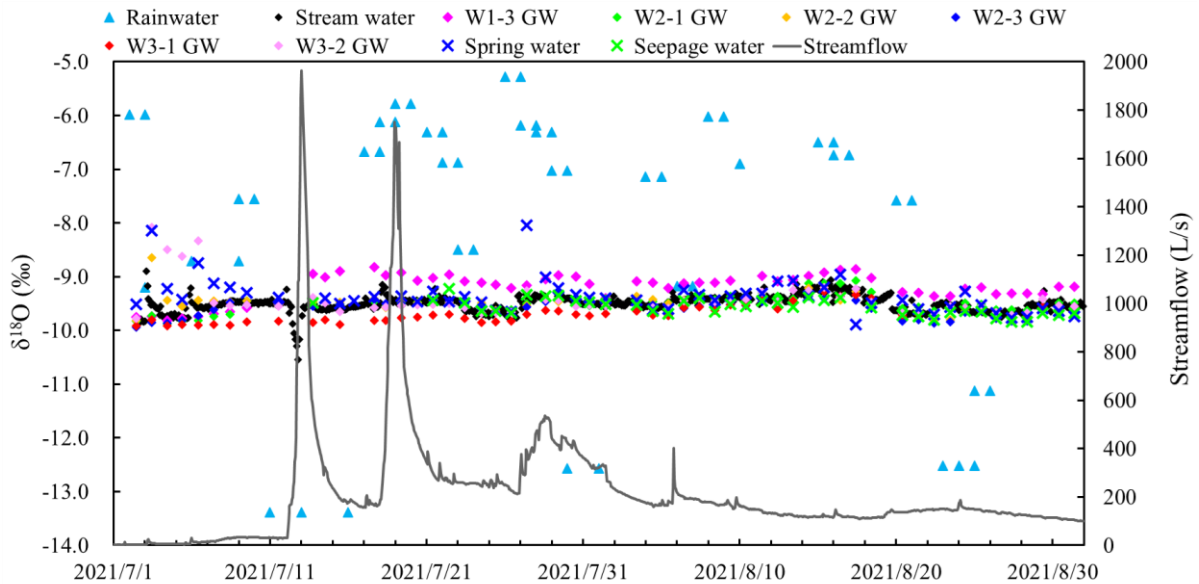
471
472 **Figure. 10.** Stable isotope $\delta^{18}O$ time series of rainwater, stream water and groundwater.

473 In Figure 11, groundwater $\delta^{18}O$ values were plotted against groundwater levels for each

474 borehole, and stream water $\delta^{18}O$ values were plotted against streamflow. The variability of

475 groundwater $\delta^{18}O$ increased with rising groundwater levels, suggesting a stronger influence of

25

476 rainwater on groundwater. Stream water's $\delta^{18}O$ remained independent of streamflow volume and

477 exhibited a range of variation similar to that of groundwater. Notably, the overlapping isotopic

478 compositions, including those during stormflow, were predominantly found in regions with higher

479 groundwater levels. This observation underscores that, even during stormflow events, groundwater

480 remains the primary source of streamflow.

481
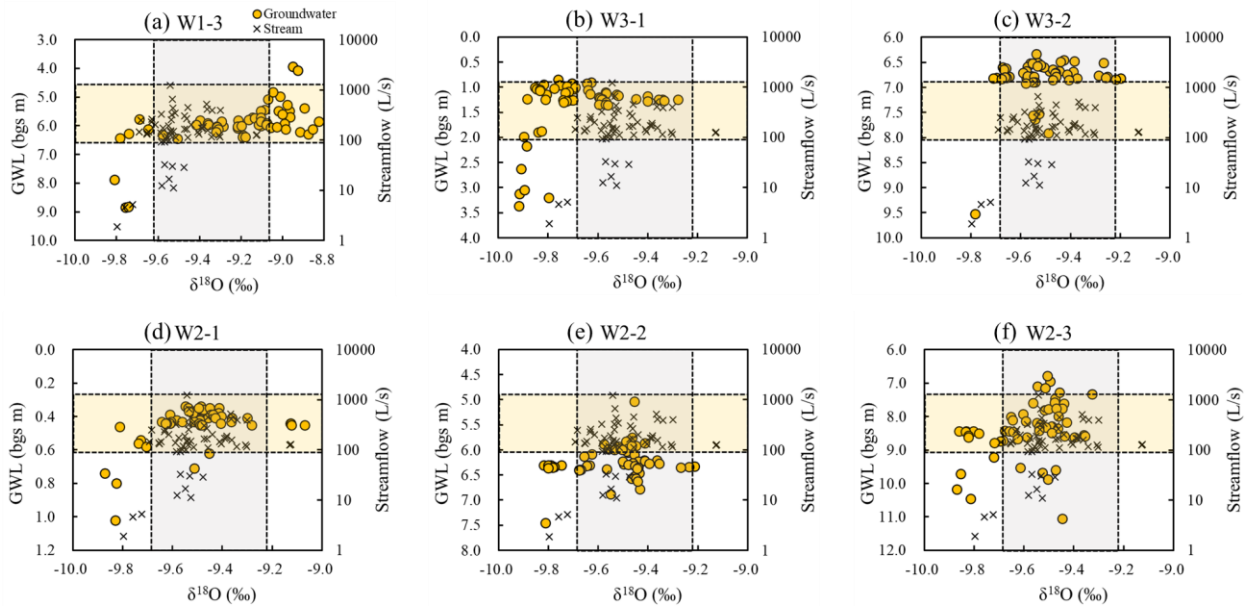
Figure 11. $\delta^{18}O$ measurements in groundwater and stream water from July 1 to September 1, 2021.
Circles and cross represent the $\delta^{18}O$ of groundwater and stream water, respectively.

4. Discussion

4.1 Lag time of delayed streamflow peaks

486   The lag time of delayed peaks varies across different water sources, providing valuable

487 insights for estimating stormflow water resources. Haga *et al.* (2005) conducted relevant studies

488 in a forested unchanneled catchment, noting that events with shorter lag times (<2 hours)

489 predominantly exhibited runoff composed of saturation excess overland flow near the spring area.

490 In contrast, events with longer lag times (>24 hours) were characterized by river runoff mainly

26

491 composed of saturated subsurface flow above the soil-bedrock interface. Becker (2005)

492 synthesized lag times from various studies in different basins, observing a trend where lag times

493 for the three main flow components differed by at least one order of magnitude, following the

494 pattern overland flow < subsurface flow < baseflow. This substantial difference in lag times is

495 likely attributed to the stochastic triggering of different flow paths by rainfall forcing in distinct

496 events.

497   Lag times for the direct streamflow peaks, observed in both unimodal and bimodal events in

498 this study, were generally within 30 minutes. These lag times exhibited no significant correlation

499 with rainfall amount, rainfall intensity, or pre-event streamflow (correlation coefficients of 0.005,

500 0.017, and 0.012, respectively). This lack of correlation suggests that the direct streamflow peaks

501 were nearly concurrent with rainfall. Therefore, we infer that these direct peaks were generated

502 either through bypass flow mechanisms, such as macropores, fractures, or soil-bedrock interfaces,

503 as interpreted in Buttle and Turcotte (1999), Onda *et al.* (2001), Uchida *et al.* (2005), and Xu *et al.*

504 (2016). Alternatively, they could have been directly contributed to the channel by rainfall. This

505 interpretation aligns with the consideration that the routing time of the river network in XEW is

506 approximately 1 hour (Zhao *et al.*, 2019).

507   In contrast to the direct peaks, the time lags from the peak rainfalls to the delayed peaks were

508 considerably longer, ranging from 5 hours to 9.9 days (Figure 3). This lag time in our study aligns

509 with findings from other studies where similar parameters were calculated (refer to Table 3). The

510 results imply that the delayed peaks observed in XEW were likely generated by subsurface flow

511 processes, as indicated in the work of Lischeid *et al.* (2002).

512

513

Table 3. Lag time between peak rainfall intensity and the delayed streamflow peak in this study and in previous studies.

| Reference	Lag time of delayed peak	The source of the delayed peak
Anderson & Burt (1978)	About one day	Subsurface flow
Onda *et al.* (2001)	Ten hours to one week	Subsurface flow and bedrock groundwater
Masiyandima *et al.* (2003)	Several hours	Subsurface flow
Becker (2005)	A day to several weeks	Subsurface stormflow
Zillgens *et al.* (2007)	Three to five days	Subsurface flow
Birkinshaw (2008)	Several tens of hours to a few days	Subsurface stormflow
Kosugi *et al.* (2011)	Two to three days	Bedrock groundwater
Fenicia *et al.* (2014)	Several hours or days	Subsurface flow
Padilla *et al.* (2014, 2015)	Within four days	Bedrock groundwater
Yang *et al.* (2015)	Several hours	Subsurface flow
This study	5 hours to 9.9 days	Subsurface flow (groundwater flow)

4.2 Hysteresis between groundwater level and streamflow

For bimodal events in XEW, the non-linear relationship between groundwater level and streamflow results in hysteretic relationships between the two variables. Figure 12 shows time series for streamflow and I_G as well as scatter plots comparing the two variables for the six events used in section 3.3. As noted by Dunne (1978), when two runoff peaks appeared in an event, there must be at least two zones in the catchment that responded to the storm and contributed to runoff. The hysteretic nature highlights the possibility of multiple hydrological compartments being active

524 and these compartments are not necessarily contributing significant flows simultaneously but

525 rather sequentially during the runoff generation period (Fovet *et al.*, 2015; Martínez-Carreras *et*

526 *al.*, 2016).

527

528
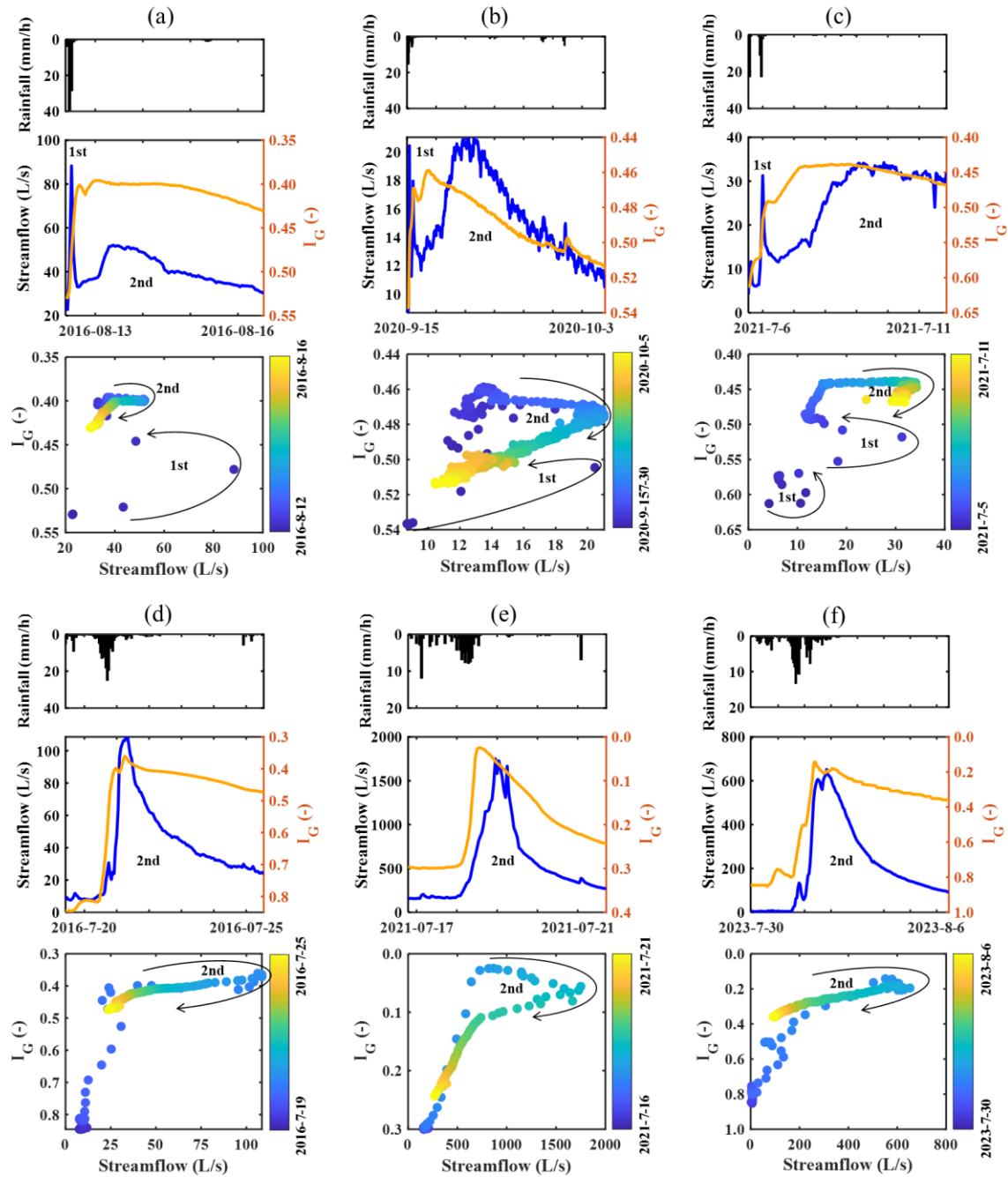
Figure 12. Streamflow and I_G with corresponding scatter plots between both variables for three typical bimodal and three hybrid bimodal events. Note that the axis scales vary between events. Arrows indicate progression of time. Direct peaks in bimodal hydrographs indicated as "1st" and delayed peaks as "2nd".

536   Streamflow increased quickly and peaked before groundwater level during direct peaks,

537   resulting in an anti-clockwise hysteretic loop. It can be explained that direct peaks were formed by

538   rainfall directly falling onto the channel or a saturation zone near the channel, and/or by the flow

539   that contributed to the channel through rapid routes, as observed in other watersheds by Jackisch

540   *et al.* (2016). In contrast, groundwater level peaked first during delayed peaks, indicating that the

541   groundwater level in the watershed peaked first and subsequently released water, creating the

542   delayed runoff peak. This behavior may be attributed to the groundwater level surpassing a

543   threshold for generating bimodal hydrographs, leading to enhanced hydraulic connectivity

544   between hillslopes and the channel. This, in turn, resulted in the swift release of a substantial

545   amount of groundwater or subsurface flow (Burt & Butcher, 1985; Detty and McGuire, 2010;

546   McGlynn & McDonnell, 2003; McGuire and McDonnell, 2010; Scaife and Band, 2017).

547   Consequently, the groundwater level is not merely a passive feature in this watershed, where

548   shallow groundwater may constitute the primary runoff component, but actively controls the

549   stormflow.

550   **4.3 Two-component hydrograph separation**

551   The two-component hydrograph separation was performed for four bimodal storm events

552   using the $\delta^{18}O$ of the bulk rainfall, a pre-event water signature (represented by the stream $\delta^{18}O$

553   before the rainfall) and the monitored stream water signature during the events. These four events

554   were chosen because their relatively complete isotope data. It should be noted that in all four

555   rainfall events, $\delta^{18}O$ values in rain and stream water were notably different, which is a requirement

556   for end-member hydrograph separation analysis. The hydrograph separation results, as well as the

557    $\delta^{18}O$ series of rainwater and stream water were shown in Figure 13.

558   Regarding the water sources separation result, these four events can be divided into two

559   groups: Event B1 and B4, the major stormflow process were lagged and considerably damped, and

560   event water contributions were higher compared to the other two events. The fraction of event

561   water comprising the hydrograph was 25% in Event B1, and the contribution ratio of event water

562   in Event 4 was 11%. Considering that the rain had already stopped, the event water component of

563   the delayed peak should be the rainwater temporarily stored in the watershed during the rainfall

564   process. Event B2 and especially Event B3, however, were almost entirely pre-event water

565   dominated (the contributions of pre-event water were 92% for Event 2 and 97% for Event B3),

566   although it was evident that some event water contributed to the stormflow during the rising and

567   peak period of streamflow, this water may have originated from the direct rainfall or rain water

568   taking a rapid route to the stream channel.

569   The hydrograph separation results indicated that the streamflow contribution of pre-event

570   water changed virtually in sync with streamflow following the onset of rain, almost entirely

571   dominating the hydrograph, while event water dominated the sharp streamflow peak responding

572   to high-intensity storm. Early in the rainy event, the pre-event component of the hydrograph

573   exceeded 50%, indicating a sufficiently swift groundwater response such that considerable

574   amounts of groundwater were released soon after the start of rain.
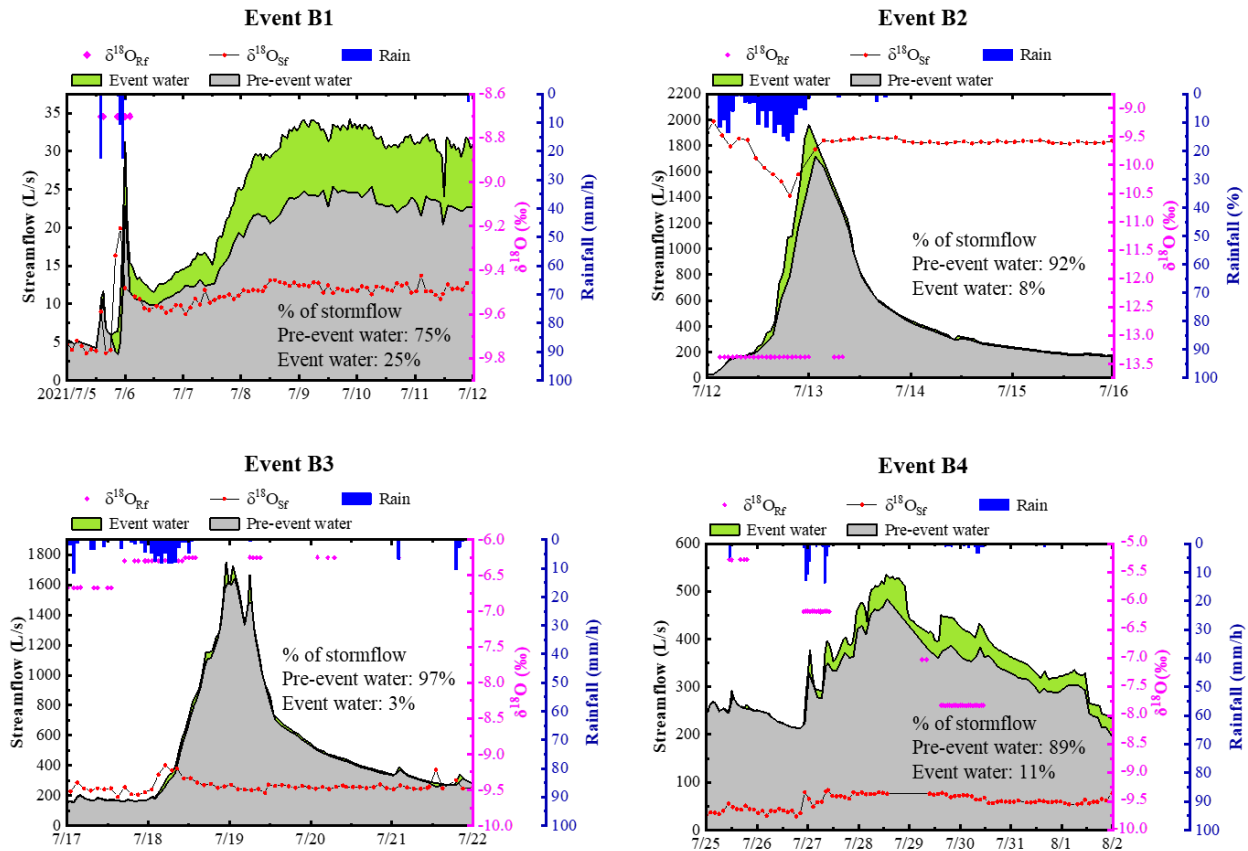
Figure 13. The partitioning of stormflow into its pre-event and event water sources using one-tracer two component hydrograph separation analysis with $\delta^{18}O$ as tracer for the four storm events. $\delta^{18}O_{Rf}$ and $\delta^{18}O_{Sf}$ are the $\delta^{18}O$ respectively for rain and stream water.

In addition, there was a noticeable, gradual rise in the pre-event water contribution to total stormflow as the catchment was wetting-up (Figure 13). Event B1 had a rather dry antecedent condition and showed a relatively lower pre-event water percentage (about 75%). Event 3 in the temporal sequence had a extremely high pre-event water proportion (approximately 97%) and occurred under highly wet antecedent conditions. In Event B4, due to a little reduced wetness condition compared to the preceding Event B3, the percentage of pre-event water decreased somewhat to approximately 89%. This pattern may be attributed to increased water flux during the wetting-up process when the water table rose into near surface soil layers with high saturated hydraulic conductivity. The rate of groundwater increase slowed as a result of the higher

588   transmissivity, and more pre-event water was mobilized and travelled rapidly to the stream via

589   shallow flow pathways (Lundin, 1982).

590   **4.4 Filed observation**

591   Our field observations on-site indicate that direct exfiltration of groundwater into the runoff

592   predominates, with few signs of hillslope overland flow. For example, during a heavy storm on

593   July 5, 2021, characterized by short duration (7 hours) and very high intensity (27.6 mm/h) with a

594   total rainfall of 65.2 mm, minimal overland flow was observed at the study site. However, post the

595   storm on July 5, the spring water flow from Hillslope 2 substantially increased. Moreover, at

596   various points in the watershed, seepage flow was observed gushing from fractures in the stone

597   and holes in the earth. These field observations strongly suggest the direct exfiltration of

598   groundwater into the runoff, providing further support to the notion that groundwater significantly

599   contributes to stormflow in the watershed.

600

601   **Figure 14.** Field observations of the spring and the seepage flows. HS1, HS2 and HS3 are Hillslope
602   1, Hillslope 2 and Hillslope 3, respectively.

603   **5. Conclusions**

604   Based on observations from 2013 to 2023, the study carried out an event-scale analysis of

605   streamflow hydrographs in a semi-humid forested watershed of North China. Three stormflow

patterns with distinct shaped hydrograph, i.e., unimodal, bimodal, and hybrid bimodal were identified. Particularly, their rainfall-runoff response characteristics as well the stormflow composition were analyzed, and derived the following conclusions:

1) Direct peaks for both unimodal and bimodal events occurred within 1 hour following the peak rainfall, while the lag time of delayed peaks ranged between 5 h and 9.9 days. The stormflow amount generated by bimodal events, due to the delayed peak, was several to hundreds of times more than that of the unimodal events, often resulting in flooding.

2) Delayed stormflow appeared when the sum of event rainfall amount (P) and antecedent soil moisture index (ASI) exceeding 200 mm. Stormflow yield is positively proportional to event peak groundwater level while the lag time of delayed peak showed an inverse correlation with peak groundwater level.

3) The isotopic analysis and two-component hydrograph separation unveiled that pre-event water predominantly contributed to the delayed stormflow, with event water dominating the sharp streamflow peak in response to high-intensity storms.

4) Streamflow peaked before groundwater level during direct peaks, suggesting that direct streamflow peaks are from direct rainfall onto the channel or rapid flow through macropores and bedrock fractures, Discharge peaked before catchment storage during single peak. But groundwater levels peaked first during delayed streamflow, suggested that the delayed stormflow is primarily made up of shallow groundwater, and this is further supported by field observation.

This study clarified the prerequisites for bimodal stormflow, and the provided information on the response characteristics and water resources of stormflow is not common knowledge for regions. We believe these findings can enrich runoff generation theory and contribute new insights for stormflow modelling in other similar regions.

35

Data availability

All the data used in this study will be available at the Zenodo website at the time of publication.

Author contribution

ZC contributed the conceptualization, formal analysis, investigation and writing; FT contributed the conceptualization, formal analysis and revision; ZZ, ZX, YD and JW contributed the Investigation; M contributed the writing.

Competing interests

Some authors are members of the editorial board of Hydrology and Earth System Sciences.

Financial support

Acknowledgments

References

Ali, G., Tetzlaff, D., McDonnell, J. J., Soulsby, C., Carey, S., Laudon, H., McGuire, K., Buttle, J., Seibert, J., and Shanley, J.: Comparison of threshold hydrologic response across northern catchments, Hydrol. Process., 29, 3575–3591, https://doi.org/10.1002/hyp.10527, 2015.

647   Anderson, M. G., and Burt, T. P.: Automatic monitoring of soil moisture conditions in a hillslope spur and

648   hollow, J. Hydrol., 33, 0–36, https://doi.org/10.1016/0022-1694(77)90096-8, 1977.

649   Anderson, M. G., and Burt, T. R.: The role of topography in controlling throughflow generation, Earth Surf.

650   Process., 3, 331–334, https://doi.org/10.1002/esp.3290030402, 1978.

651   Becker, A.: Runoff Processes in Mountain Headwater Catchments: Recent Understanding and Research

652   Challenges, in: Global Change and Mountain Regions, 283–295, https://doi.org/10.1007/1-4020-3508-

653   x_29, 2005.

654   Becker, A., and McDonnell, J. J.: Topographical and ecological controls of runoff generation and lateral flows

655   in mountain catchments, IAHS Publ., 248, 199-206, 1998.

656   Birkinshaw, S. J.: Physically‑based modelling of double‑peak discharge responses at Slapton Wood

657   catchment, Hydrol. Process., 22, 1419–1430, https://doi.org/10.1002/hyp.6694, 2008.

658   Burt, T. P., and Butcher, D. P.: Topographic controls of soil moisture distributions, J. Soil Sci., 36, 469–486,

659   https://doi.org/10.1111/j.1365-2389.1985.tb00351.x, 1985.

660   Buttle, J. M., Dillon, P. J., and Eerkes, G. R.: Hydrologic coupling of slopes, riparian zones and streams: An

661   example from the Canadian Shield, J. Hydrol., 287, 161–177, https://doi.org/10.1016/j.jhydrol.2003.09.022,

662   2004.

663   Buttle, J. M., and Turcotte, D. S.: Runoff processes on a forested slope on the Canadian Shield, Hydrol. Res.,

664   30, 1-20, https://doi.org/10.1016/S0304-2995(99)80027-8, 1999.

665   Detty, J. M., and Mcguire, R. J.: Threshold changes in storm runoff generation at a till-mantled headwater

666   catchment, Water Resour. Res., 46, 759–768, https://doi.org/10.1029/2009wr008102, 2010.

667   Dingman, S. L.: Physical hydrology, Waveland Press, Long Grove, IL, 2015.

668   Dubreuil, P. L.: Etude hydrologique de petits bassins en Cote d'Ivoire, Rapport general, ORSTOM Service

669   Hydrologique, 1960.

670   Dubreuil, P. L.: Review of field observations of runoff generation in the tropics, J. Hydrol., 80, 237–264,

671   https://doi.org/10.1016/0022-1694(85)90119-2, 1985.

672   Dunne, T.: Field studies of hillslope flow processes, in: Hillslope Hydrology, edited by: Kirkby, M. J., Wiley,

673   London, 227–293, 1978.

674   Fenicia, F., Kavetski, D., Savenije, H. H., Clark, M. P., Schoups, G., Pfister, L., and Freer, J.: Catchment

675   properties, function, and conceptual model representation: is there a correspondence?, Hydrol. Process., 28,

676   2451–2467, https://doi.org/10.1002/hyp.9726, 2014.

677   Fovet, O., Ruiz, L., Hrachowitz, M., Faucheux, M., and Gascuel-Odoux, C.: Hydrological hysteresis and its

678   value for assessing process consistency in catchment conceptual models, Hydrol. Earth Syst. Sci., 19, 105-

679   123, https://doi.org/10.5194/hess-19-105-2015, 2015.

680   Fu, C., Chen, J., Jiang, H., and Dong, L.: Threshold behavior in a fissured granitic catchment in southern China:

681   1. Analysis of field monitoring results, Water Resour. Res., 49, 2519–2535,

682   https://doi.org/10.1002/wrcr.20191, 2013.

683   Graeff, T., Zehe, E., Reusser, D., Lück, E., Schröder, B., Wenk, G., John, H., and Bronstert, A.: Process

684   identification through rejection of model structures in a mid-mountainous rural catchment: observations of

685   rainfall-runoff response, geophysical conditions and model inter-comparison, Hydrol. Process., 23, 702–

686   718, https://doi.org/10.1002/hyp.7171, 2009.

687   Gu, W.: On the hydrograph separation traced by environmental isotopes, Adv. Water Sci., 7, 105–111, 1996.

688   Haga, H., Matsumoto, Y., Matsutani, J., Fujita, M., Nishida, K., and Sakamoto, Y.: Flow paths, rainfall properties,

689   and antecedent soil moisture controlling lags to peak discharge in a granitic unchanneled catchment, Water

690   Resour. Res., 41, 2179–2187, https://doi.org/10.1029/2005wr004236, 2005.

691   Iwagami, S., Tsujimura, M., Onda, Y., Shimada, J., and Tanaka, T.: Role of bedrock groundwater in the rainfall-

692   runoff process in a small headwater catchment underlain by volcanic rock, Hydrol. Process., 24, 2771–2783,

693   https://doi.org/10.1002/hyp.7690, 2010.

694   Jackisch, C., Angermann, L., Allroggen, N., Sprenger, M., Blume, T., Weiler, M., Tronicke, J., and Zehe, E.: In

695   situ investigation of rapid subsurface flow: identification of relevant spatial structures beyond heterogeneity,

696   Hydrol. Earth Syst. Sci. Discuss., 1–32, https://doi.org/10.5194/hess-2016-190, 2016.

697

698 Jenkins, A., Ferrier, R. C., Harriman, R., and Ogunkoya, Y. O.: A case study in catchment hydrochemistry:

699   Conflicting interpretations from hydrological and chemical observations, Hydrol. Process., 8, 335–349,

700   https://doi.org/10.1002/hyp.3360080406, 1994.

701 Kosugi, K., Fujimoto, M., Katsura, S., Kato, H., Sando, Y., and Mizuyama, T.: Localized bedrock aquifer

702   distribution explains discharge from a headwater catchment, Water Resour. Res., 47,

703   https://doi.org/1029/2010WR009884, 2011.

704 Lischeid, G., Kolb, A., and Alewell, C.: Apparent translatory flow in groundwater recharge and runoff generation,

705   J. Hydrol., 265, 195–211, https://doi.org/10.1016/s0022-1694(02)00108-7, 2002.

706 Lundin, L.: Soil moisture and ground water in till soil and the significance of soil type for runoff, PhD Thesis,

707   Uppsala University, UNGI Report, 56, 216, 1982.

708 Martínez-Carreras, N., Hissler, C., Gourdol, L., Klaus, J., Juilleret, J., Iffly, J. F., and Pfister, L.: Storage controls

709   on the generation of double peak hydrographs in a forested headwater catchment, J. Hydrol., 543, 255–269,

710   https://doi.org/10.1016/j.jhydrol.2016.10.004, 2016.

711 Martínez-Carreras, N., Wetzel, C. E., Frentress, J., Ector, L., McDonnell, J. J., Hoffmann, L., and Pfister, L.:

712   Hydrological connectivity inferred from diatom transport through the riparian-stream system, Hydrol. Earth

713   Syst. Sci., 19, 3133–3151, https://doi.org/10.5194/hess-19-3133-2015, 2015.

714 Masiyandima, M. C., van de Giesen, N., Diatta, S., Windmeijer, P. N., and Steenhuis, T. S.: The hydrology of

715   inland valleys in the sub-humid zone of West Africa: rainfall-runoff processes in the M'be experimental

716   watershed, Hydrol. Process., 17, 1213–1225, https://doi.org/10.1002/hyp.1191, 2003.

717 McDonnell, J. J., Bonell, M., Stewart, M. K., and Pearce, A. J.: Deuterium variations in storm rainfall:

718   Implications for stream hydrograph separation, Water Resour. Res., 26, 455–458,

719   https://doi.org/10.1029/WR026i003p00455, 1990.

720 McDonnell, J. J., Sivapalan, M., Vaché, K., Dunn, S., Grant, G., Haggerty, R., Hinz, C., Hooper, R., Kirchner,

721   J., Roderick, M. L., Selker, J., and Weiler, M.: Moving beyond heterogeneity and process complexity: A

722   new vision for watershed hydrology, Water Resour. Res., 43, https://doi.org/10.1029/2006WR005467,

723   2007.

McGlynn, B. L., and McDonnell, J. J.: Quantifying the relative contributions of riparian and hillslope zones to catchment runoff, Water Resour. Res., 39, 1310, https://doi.org/10.1029/2003wr002091, 2003.

McGuire, K. J., and McDonnell, J. J.: Hydrological connectivity of hillslopes and streams: Characteristic time scales and nonlinearities, Water Resour. Res., 46, https://doi.org/10.1029/2010WR009341, 2010.

Mosley, M. P.: Streamflow generation in a forested watershed, New Zealand, Water Resour. Res., 15, 795–806, https://doi.org/10.1029/wr015i004p00795, 1979.

Onda, Y., Komatsu, Y., Tsujimura, M., and Fujihara, J.: The role of subsurface runoff through bedrock on storm flow generation, Hydrol. Process., 15, 1693–1706, https://doi.org/10.1002/hyp.234, 2001.

Padilla, C., Onda, Y., Iida, T., Takahashi, S., and Uchida, T.: Characterization of the groundwater response to rainfall on a hillslope with fractured bedrock by creep deformation and its implication for the generation of deep-seated landslides on Mt. Wanitsuka, Kyushu Island, Geomorphology, 204, 444–458, https://doi.org/10.1016/j.geomorph.2013.08.024, 2014.

Padilla, C., Onda, Y., and Iida, T.: Interaction between runoff-bedrock groundwater in a steep headwater catchment underlain by sedimentary bedrock fractured by gravitational deformation, Hydrol. Process., 29, 4398–4412, https://doi.org/10.1002/hyp.10498, 2015.

Penna, D., Tromp-van Meerveld, H. J., Gobbi, A., Borga, M., and Dalla Fontana, G.: The influence of soil moisture on threshold runoff generation processes in an alpine headwater catchment, Hydrol. Earth Syst. Sci., 15, 689–702, https://doi.org/10.5194/hess-15-689-2011, 2011.

Phillips, J. D.: Sources of nonlinearity and complexity in geomorphic systems, Prog. Phys. Geogr., 27, 1–23, https://doi.org/10.1191/0309133303pp340ra, 2003.

Powell, D. N., Khan, A. A., Aziz, N. M., and Raiford, J. P.: Dimensionless rainfall patterns for South Carolina, J. Hydrol. Eng., 12, 130–133, https://doi.org/10.1061/(asce)1084-0699(2007)12:1(130), 2007.

Ross, C. A., Ali, G. A., Spence, C., and Courchesne, F.: Evaluating the Ubiquity of Thresholds in Rainfall-Runoff Response Across Contrasting Environments, Water Resour. Res., 57, e2020WR027498, https://doi.org/10.1029/2020wr027498, 2021.

749   Scaife, C. I., and Band, L. E.: Nonstationarity in threshold response of stormflow in southern Appalachian

750   headwater catchments, Water Resour. Res., 53, 6579–6596, https://doi.org/10.1002/2017WR020376, 2017.

751   Sivapalan, M.: Process complexity at hillslope scale, process simplicity at the watershed scale: Is there a

752   connection?, Hydrol. Process., 17, 1037–1041, https://doi.org/10.1002/hyp.5109, 2003.

753   Sloto, R. A., and Crouse, M. Y.: HYSEP: A computer program for streamflow hydrograph separation and

754   analysis, US Geol. Surv., https://doi.org/10.3133/wri964040, 1996.

755   Tian, F., Li, H., and Sivapalan, M.: Model diagnostic analysis of seasonal switching of runoff generation

756   mechanisms   in   the   blue   river   basin,   Oklahoma,   J.   Hydrol.,   418-419,   136–149,

757   https://doi.org/10.1016/j.jhydrol.2010.03.011, 2012.

758   Tie, Q., Hu, H., Tian, F., Guan, H., and Lin, H.: Environmental and physiological controls on sap flow in a

759   subhumid   mountainous   catchment   in   north   China,   Agric.   For.   Meteorol.,   240–241,   46–57,

760   https://doi.org/10.1016/j.agrformet.2017.03.018, 2017.

761   Tromp-van Meerveld, H. J., and McDonnell, J. J.: Threshold relations in subsurface stormflow: 1. A 147-storm

762   analysis of the Panola hillslope, Water Resour. Res., 42, W02410, https://doi.org/10.1029/2004WR003778,

763   2006.

764   Uchida, T., Tromp-van Meerveld, I., and McDonnell, J. J.: The role of lateral pipe flow in hillslope runoff

765   response: An intercomparison of non-linear hillslope response, J. Hydrol., 311, 117–133,

766   https://doi.org/10.1016/j.jhydrol.2005.01.012, 2005.

767   Westhoff, M. C., Bogaard, T. A., and Savenije, H. H. G.: Quantifying spatial and temporal discharge dynamics

768   of an event in a first order stream, using distributed temperature sensing, Hydrol. Earth Syst. Sci., 15, 1945-

769   1957, https://doi.org/10.5194/hess-15-1945-2011, 2011.

770   Weyman, D. R.: Throughflow on hillslopes and its relation to the stream hydrograph, Int. Assoc. Sci. Hydrol.

771   Bull., 15, 25–33, https://doi.org/10.1080/02626667009493969, 1970.

772   Wrede, S., Fenicia, F., Martínez-Carreras, N., Juilleret, J., Hissler, C., Krein, A., Savenije, H. H. G., Uhlenbrook,

773   S., Kavetski, D., and Pfister, L.: Towards more systematic perceptual model development: a case study

774   using 3 Luxembourgish catchments, Hydrol. Process., 29, 2731–2750, https://doi.org/10.1002/hyp.10393,

775   2015.

776 Xu, Q., Liu, H., Ran, J., Li, W., and Sun, X.: Field monitoring of groundwater responses to heavy rainfalls and

777   the early warning of the Kualiangzi landslide in Sichuan Basin, southwestern China, Landslides, 13, 1555-

778   1570, https://doi.org/10.1007/s10346-016-0717-3, 2016.

779 Yang, Y., Endreny, T. A., and Nowak, D. J.: Simulating double-peak hydrographs from single storms over

780   mixed-use watersheds, J. Hydrol. Eng., 20, 06015003, https://doi.org/10.1061/(ASCE)HE.1943-

781   5584.0001225, 2015.

782 T., Wang, J., Tang, J. B., Chen, R., and Lei, M. Y.: Stormflow generation in a humid forest watershed controlled

783   by antecedent wetness and rainfall amounts, J. Hydrol., 603, https://doi.org/10.1016/j.jhydrol.2021.127107,

784   2021.

785 Zillgens, B., Merz, B., Kirnbauer, R., and Tilch, N.: Analysis of the runoff response of an alpine catchment at

786   different scales, Hydrol. Earth Syst. Sci., 11, 1441–1454, https://doi.org/10.5194/hess-11-1441-2007, 2007.

787

Appendix A: Supplementary Figures of Results and discussion
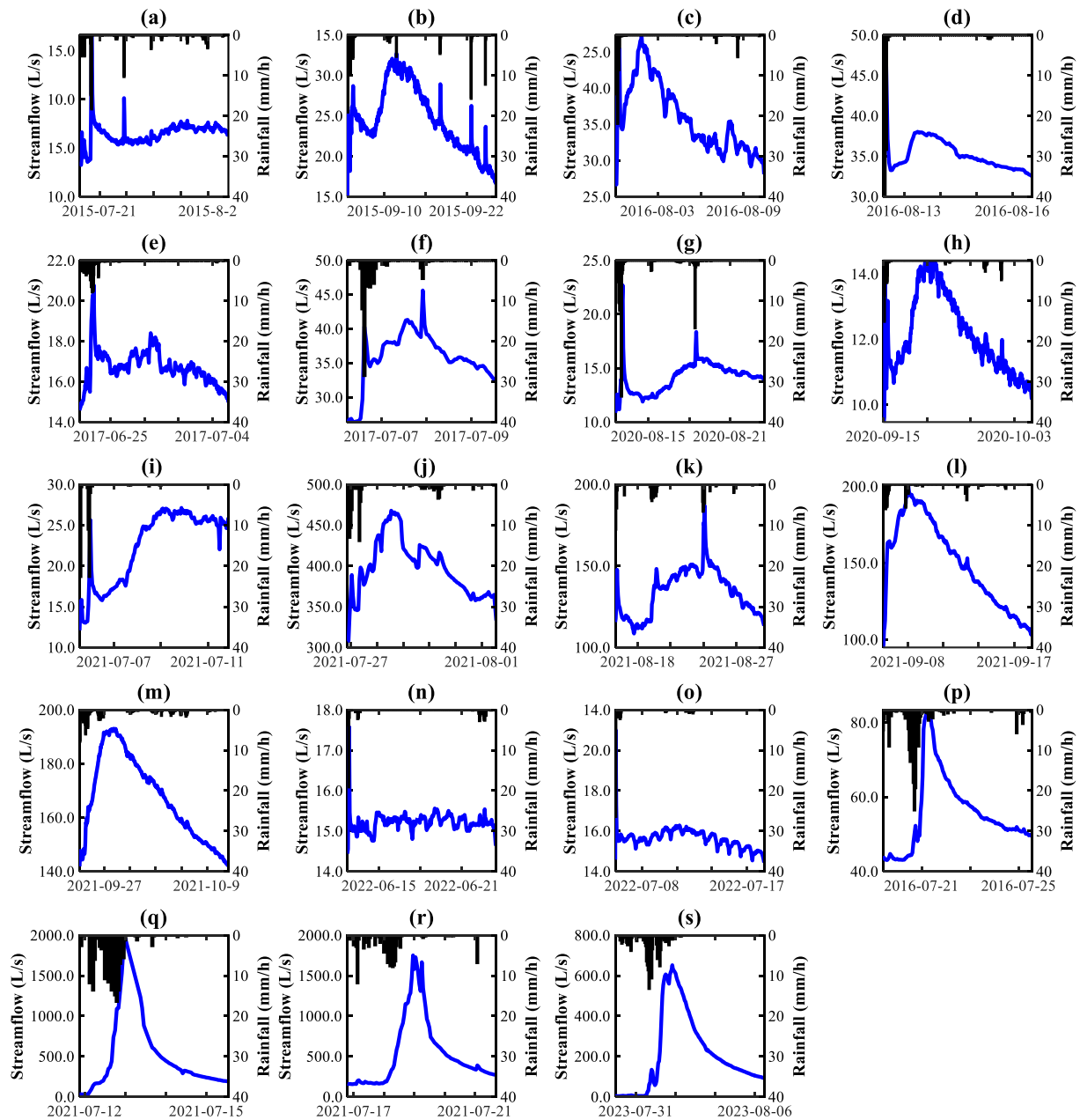
789
Figure A1. Rainfall and streamflow hydrograph for (a-o) 15 bimodal and (p-s) 4 hybrid bimodal
events.